Proceedings of IMECE 2011
2011 ASME International Mechanical Engineering Congress and Exposition
November 11-17, 2011, Denver, Colorado, USA

DRAFT IMECE2011-63281

SHEAR/PRESSURE DRIVEN INTERNAL CONDENSING FLOWS AND THEIR SENSITIVITY TO INLET PRESSURE FLUCTUATIONS

M. Kivisalu, N. Gorgitrattanagul, S. Mitra, R. Naik, and A. Narain
Department of Mechanical Engineering-Engineering Mechanics
Michigan Technological University, Houghton, MI 49931
Email: narain@mtu.edu

Abstract: The reported experimental results are for *annular zones* of *fully condensing* flows of pure FC-72 vapor. The flow condenses on the horizontal condensing surface (316 stainless steel) which is the bottom surface (wall) of a rectangular cross-section duct of 2 mm height, 15 mm width, and 1 m length. The sides and top of the duct are made of clear plastic. The experimental system in which this condenser is used is able to control steady-in-the-mean (termed quasi-steady) values of mass flow rate, inlet (or exit) pressure, and wall cooling conditions. Earlier it has been reported that, with the condenser mean (time averaged) inlet mass flow rate, mean inlet (or exit) pressure, and wall cooling condition held at steady values, there is a very strong sensitivity to certain impositions of pressure fluctuations and accompanying flow rate pulsations at the condenser inlet. For these certain impositions, it was found that the mean exit (or inlet) pressure changes to significantly affect mean test-section pressure difference, local heat-flux variations over the annular portion of the flow, and the nature of the annular flow regime. This paper experimentally investigates how the strength of this sensitivity varies with amplitude and frequency of pressure fluctuations imposed on the inlet of the condenser from the vapor line. It has been found that, for various frequencies of interest, there are typically two classes of responses to inlet pressure fluctuations. These are termed *supercritical* (for the larger amplitudes for which a strong sensitivity exists) and *subcritical* (for the smaller amplitudes for which a weak sensitivity exists).

Keywords: horizontal channel condensation, fluctuation sensitivity, internal condensing flows, flow pulsation

1. Introduction:

This paper presents a fundamental experimental investigation of a shear/pressure driven internal condensing flow's quasi-steady pressure-difference sensitivity to the amplitude and frequency of pressure fluctuations (and flow pulsations) imposed at the inlet of the condenser. Inadvertently or deliberately, such imposed fluctuations frequently occur in closed flow loops in which the condensing flow is primarily shear driven and devices like turbines or reciprocating compressors introduce significant pressure pulsations to the vapor supplied to the condenser. Imposed pressure fluctuation cases reported here extend the results reported earlier in Kivisalu et al. [1] by considering a range of amplitudes and frequencies. It should be noted that pressure pulsation amplitudes on the order of 100 - 1000 Pa (for a representative mean inlet pressure range of 50 - 200 kPa) induce large pulsations in the inlet mass flow rate. Note that, the pressure difference across the annular length of many mm-scale (or higher) hydraulic diameter condensers are often, themselves, of the order of 100 – 1000 Pa. Therefore, the pressure fluctuation amplitudes imposed at the inlet significantly affect the annular flow condensation.

Shear/pressure driven internal condensing flows are of interest here because they occur in horizontal ducts, micro-gravity, and micro-meter scale hydraulic diameter ducts. These conditions are of interest for next generation space

based thermal management systems and high power electronic cooling applications.

For assistance in the development of predictive abilities for condensing flows, there are many experimental papers that deal with condensation of pure vapors flowing inside vertical or horizontal ducts (of circular or rectangular cross-sections, as in Goodykoontz and Dorsch [2], Cavallini and Zechchin [3], etc.). The experiments as well as related correlations (Shah [4], Cavallini et al. [5], etc.) in the literature typically cover a large set of flow regimes and associated flow physics categories (see Mitra et al. [6] and Kurita et al. [7]).

The new experimental results reported here complement recently reported (Kulkarni et al. [8]) theoretical results. Shear/pressure driven flows, as compared to gravity driven flows, are much more sensitive and need very different specifications and control of inlet/exit conditions to ensure that the experimental data are meaningful and repeatable. For example, as shown in Kurita et al. [7], gravity driven condensate motion for condensing flows do not show any significant sensitivity to the imposition of reported levels of fluctuations on the inlet pressure or inlet flow rate. Furthermore, for gravity driven flows, if mean inlet flow rate, mean inlet (or exit) pressure, and cooling conditions are specified and steady, the pressure-difference across the duct is well defined, and no other mean pressure-difference arises, even in the presence of significant pressure pulsations at the condenser inlet as reported in Kurita et al. [7]. However, this paper shows that, shear/pressure driven fully condensing flows' quasi-steady realization under quasi-steady prescriptions of mean inlet flow rate, one of the mean boundary pressures (exit or inlet), and cooling conditions for the condensing-surface is not sufficient, by itself, to ensure their repeatability unless amplitudes of fluctuations in the inlet vapor pressure (and associated flow rates) over a relevant range of frequencies are known. This paper shows that if the amplitudes of inlet pressure fluctuations are above a critical value, the resulting quasi-steady flow's characteristics (in heat flux and flow morphology) are significantly different from those associated with negligible or subcritical amplitudes

The inlet pressure fluctuation sensitivity reported here for fully condensing flows and supporting theoretical/computational work (not reported here for brevity) correct our results reported in Kulkarni et al. [8]. These results may also be a factor in understanding the variety of complex flow morphologies (Wu and Cheng [9], Coleman and Garimella [10], etc.) and transient phenomena (Wedekind and Bhatt [11], etc.) that are possible for shear/pressure driven flow condensation. A similar result is expected to hold for flow boiling, and our group is currently establishing this experimentally. These sensitivities for flow boiling will be helpful in understanding flow transients and instabilities (Brutin et al. [12], Kandlikar [13], etc.) that are known to be present for shear/pressure driven micro-scale flow boiling.

New computational results in support of the quantitative experimental results reported here for quasi-steady shear/pressure driven condensing flows in a horizontal channel of rectangular cross-section will be reported elsewhere and are not reported here for brevity.

The reported results advance prediction and control capabilities for shear driven internal condensing flows in the context of their unique sensitivities to inadvertent or deliberate impositions of fluctuations / pulsations on the mean values of inlet pressure or flow rate.

The above identified sensitivity results for quasi-steady annular flow condensation (in conjunction with analogous results for flow boiling) is important to the development of promising new designs of vapor compression cycles (for micro-scale, space, or aircraft applications) that exploit this sensitivity to keep the condenser and the boiler operating in the annular regime under high heat-flux conditions.

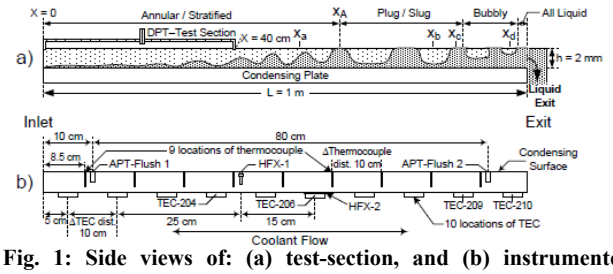

Fig. 1: Side views of: (a) test-section, and (b) instrumented condensing plate

Nomenclature:

a: amplitude of inlet pressure fluctuations

f: frequency of inlet pressure fluctuations

$\overline{T}_w$**:** time-averaged (mean) wall temperature of condenser

ΔP: pressure difference across entire length of condenser unless specified otherwise by subscripts (Pa or kPa)

$\dot{M}_{in}$**:** mass flow rate of vapor supplied to condenser (g/s)

h_{fg}**:** enthalpy of vaporization working fluid in condenser (kJ/kg)

p: pressure (kPa)

p^*_{in}: inlet pressure feedback control set point (kPa)
PID: proportional-integral-derivative (of feedback control)
t: time (seconds or minutes)
T_{bath}: temperature of water surrounding evaporator in Fig. 2 (deg C)
TEC: solid state electronic heat pump
x: distance from condenser inlet in direction of flow (cm)
x_A: length of annular flow regime in condenser (cm), see Fig. 1a

Subscripts:
in: at condenser inlet
exit: at condenser exit
p-in: inlet pressure related
NF: associated with a no-fluctuation condensing flow
IF: associated with a imposed-fluctuation condensing flow
IF-LA: associated with low amplitude imposed-fluctuation condensing flow
IF-HA: associated with high amplitude imposed-fluctuation condensing flow
0–4: over the first 40 cm of the condenser length

2. Experimental Set -up

2.1 Description

Fully condensing flows of FC-72 vapor in a horizontal rectangular cross-section (2 mm gap height and 15 mm wide) duct of 1 m length are investigated. Its horizontal condensing surface area (15 mm x 1 m) is the top of a 12.7 mm thick stainless steel plate. The channel's top and side surfaces are made of a thick transparent material (lexan), which is covered with an insulation that can be removed to allow flow visualization.

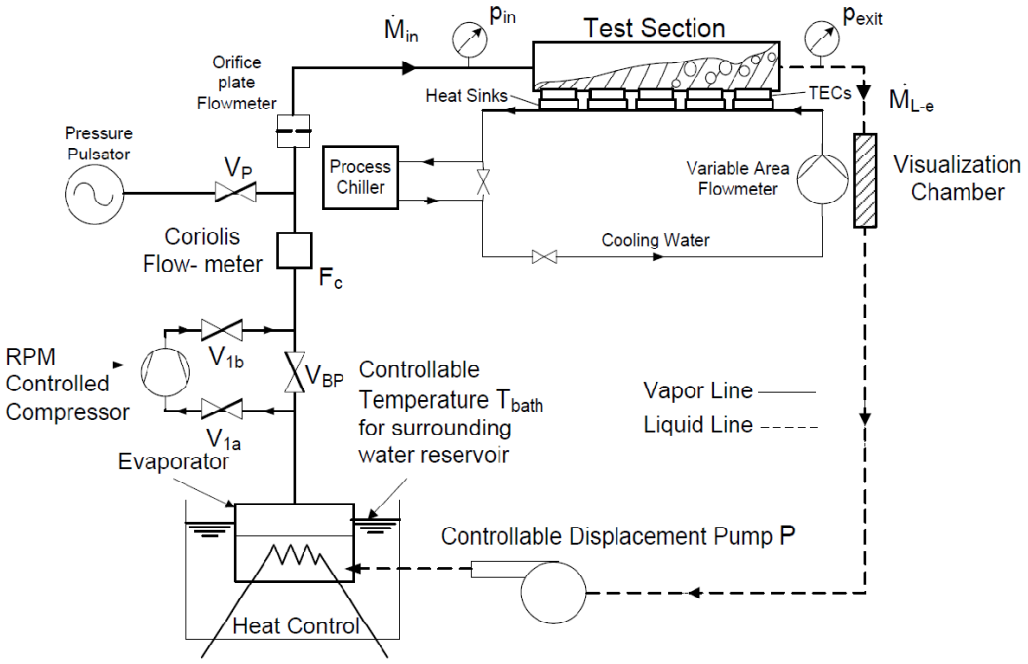

Fig. 2: Schematic of the experimental flow-loop

Transport and thermodynamic fluid properties of FC-72 are available from 3M Corporation. This choice of fluid is for safety of operations under laboratory conditions at a university.

The flow-loop in Fig. 2 has three independent feedback control strategies that can fix steady-in-the-mean values of: inlet mass flow rate $\bar{\dot{M}}_{in}$, condensing-surface cooling conditions, and exit (or inlet) pressure. Mean inlet mass flow rate, $\bar{\dot{M}}_{in}$, is fixed through active feedback control of the power input to the electric heater inside the evaporator / boiler. Evaporator pressure is stabilized using the surrounding water reservoir temperature. Condensing-surface temperature $\bar{T}_w(x)$ is obtained for a fully specified steady cooling approach that results from a specified temperature and flow rate for the flowing coolant water where it first approaches the condensing plate's heat sinks. The cooling approach may further be specified depending on whether or not additional and specified cooling conditions from feedback controlled thermoelectric coolers (TECs), which are on the bottom surface of the condensing-plate (Fig. 1b) and reject heat into the flow of cooling water, are used. Either the mean exit pressure $\bar{p}_{exit}$ or the mean inlet pressure $\bar{p}_{in}$ is held fixed by active feedback control of the controllable displacement pump P. When mean

exit pressure $\bar{p}_{exit}$ was held fixed by the pump P (as in Kivisalu et al. [1] and additional experiments which will be reported elsewhere), fixing of different mean inlet pressure $\bar{p}_{in}$ values was attempted through control of the rpm of the muffled compressor C (which has negligible pressure fluctuations at its exit). The pulsator (a frequency controlled diaphragm compressor, which is used after removing the valves between its suction and compression chambers) downstream of the Coriolis meter F_c cannot change the mean flow rate but is able to provide an independent control on pressure and mass flow rate fluctuations present at the test-section inlet, with frequency being controlled by the pulsator speed and amplitude being controlled by valve V_P.

A 0 - 300 W electric ring heater inside the evaporator/boiler in Fig. 2 causes the working fluid (FC - 72) to evaporate and/or experience nucleate boiling near the heater surface. The mean vapor mass flow rate out of the evaporator, $\dot{M}_{in}$, is fed into the test section. This mass flow rate is measured by a Coriolis flow meter F_c. The mean F_c value is used and brought to a steady set-point value by a feedback controlled heating of the evaporator through a PID control implemented in LabVIEW. Downstream of the evaporator, in the indicated bypass loop, there is an oil-free, semi-hermetically sealed compressor (which is a positive displacement vane type compressor with four graphite vanes) which is magnetically coupled to an rpm controlled motor. The purpose of the compressor is to test whether changes in compressor rpm (and/or changing the opening in the valve V_{BP} in the bypass loop) can be used to change the test-section pressure difference (i.e. change inlet pressure while holding the mean test-section exit pressure approximately fixed). If this is not possible, changes in pressure difference across the compressor will only change the boiler/evaporator pressure and/or the inlet vapor mass flow rate. The sealed enclosure for the compressor is such that it effectively removes all 0-50 Hz frequencies (this is the frequency range of interest for investigating the condenser response) in the pressure fluctuations downstream of the compressor. Since changes in the test-section pressure difference may, alternatively, be affected by the amplitude and frequency content of the superposed time-periodic pressure fluctuations at the inlet of the test-section, a pressure pulsator is introduced and located downstream of F_c in Fig. 2.

The flow of coolant water in Fig. 2 (also see Kurita et al. [7]) is supplied with the help of a commercially available process chiller and a manually adjusted value of the water flow rate (0-17 liters/min). This closed loop assures that the coolant (water) flow supplied to the test section heat sinks has a specified steady bulk mean temperature (at a fixed location) and steady flow rate. In addition to this traditional cooling approach, as shown in Fig. 1b, various TECs are located in the condensing plate. Each of the TECs can be separately activated and controlled for any additional cooling need.

2.2 Instrumentation

Kulite flush-type absolute pressure-transducers are used in the test-section at locations 10 and 90 cm downstream of the inlet of the test section. Their accuracies, after calibration, are ± 0.7 kPa. Four high accuracy pressure transducers from Omega Engineering are used to measure upstream and downstream absolute pressures for the orifice meter and the condenser. Their accuracies, after calibration, are ± 0.2 kPa for the test-section transducers and ± 0.5 kPa for the transducers across the orifice meter in Fig. 2. The accuracies of the other pressure transducers in the system are approximately ± 0.6 kPa. The differential pressure transducer used for the test-section, across locations shown in Fig. 1a, is from Validyne Inc. It is a variable-reluctance type transducer with an accuracy, after calibration, of ± 20 Pa. Temperatures are measured by T-type thermocouples with accuracies, after calibration, lying within ± 1^{o}C. The heat flux meter HFX-1 (from Vatell Corporation) in Fig. 1b has an accuracy of approximately ±7.2% of its reading, in W/cm^{2}, and an approximate range of 0-10 W/cm^{2} when used with our existing amplifier and data acquisition system. The mean mass flow rate measured from the Coriolis Meter F_c in Fig. 2 is accurate up to ±0.35% of flow, or within ± 0.007 g/s for the range of flow rates (0-2 g/s) investigated here. The orifice plate meter in Fig. 2 is our own design, and its dynamic pressure difference signal, in conjunction with computational fluid dynamic analysis and empirical correction factors obtained from suitable calibration experiments, can yield approximate estimates of the time-varying values of mass flow rates fluctuating around a steady mean. Only the steady mean mass flow rate can be obtained from the Coriolis meter F_c readings as the device cannot resolve the frequencies of interest for dynamic data acquisition.

For typical reporting of mean quasi-steady data of all

variables over minutes to hours, the National Instruments' (NI) data acquisition system is used and data is acquired at approximately 1.1 s intervals. The same variables' dynamic data are acquired every 0.5 ms over occasional 5 s intervals. Together, the two rates of data acquisitions reliably yield the signals' frequency content over 0 - 1000 Hz. The data acquisition devices used to acquire data at 1 s intervals and run the feedback controls are NI's PCI6251 card, used with their SCXI-1000 chassis in which are one SCXI-1102 module, one SCXI-1102B module, and two SCXI-1124 modules. The thermocouples are all run through the SCXI-1102 module; the pressure, flow, and heat flux transducers are all run through the SCXI-1102B module. The TECs (0 - 20 mA), compressor (0 - 10 V), and pulsator (0 - 10 V) output signals are run through the SCXI-1124 modules. The dynamic data are acquired using the NI USB-6211 data acquisition platform. The electrical signal output for control of pumps (0 - 10 V analog) and relays (5 V variable width and frequency pulse train) are also run through the USB-6211 system at this 1.1 s data acquisition rate. The still pictures and video are taken with a Nikon Coolpix P500 camera that is mounted on a suitably located track.

2.3 Cooling Conditions and Procedure

The condensing surface's cooling approach (which defines its thermal boundary condition) consists of:

(i) Coolant water flows through heat sinks under the 12.7 mm thick condensing plate at a controlled steady flow rate (0.46 m^3 / hr) and inlet temperature (24 ^oC).

(ii) Two thermo-electric coolers, namely TEC-4 removing heat from an effective area of approximately 30 cm $\leq x \leq$ 40 cm, and TEC-6 removing heat from an effective area of approximately 50 cm $\leq x \leq$ 60 cm (see Fig. 1b) are PID controlled at 45 ^oC using the thermocouples at x = 38.5 cm and x = 48.5 cm respectively. For some of the cases in Table 1, TEC-6 was unable to hold the wall temperature at x = 48.5 cm to 45 ^oC, so it runs at full power (20 – 22 V) similar to TEC-9 and TEC-10 described below.

(iii) The thermo-electric coolers (TEC-9 and TEC-10 in Fig. 1b), removing heat from the approximate region of 80 cm $\leq x \leq$ 1 m, are operated at a fixed driving voltage (10 V) to ensure that the subsequent flow morphology changes rapidly to an all liquid flow by the exit of the test-section.

The above described cooling approaches (with the rest of the TECs being off) define the condensing-surface thermal boundary conditions. A similar steady cooling approached was used in Kivisalu et al. [1]. These cooling approaches are mathematically defined and modeled in Kulkarni et al. [8].

2.4 Procedures

2.4.1 No-Fluctuation Steady/Quasi-Steady Flows

The procedure is for achieving steady/quasi-steady natural (i.e. without fluctuations at the inlet) fully condensing flows whose effective point of full condensation is within the test-section. Downstream of the exit (including the Visualization Chamber in Fig. 2), the flow loop is all liquid up to the evaporator. This procedure involves: (i) keeping the compressor and the pulsator off with the bypass valve (V_{BP} in Fig. 2) fully open, (ii) fixing the evaporator bath temperature T_{bath}, (iii) holding fixed the Coriolis mass flow meter F_c (in Fig. 2) reading of the mass flow rate $\overline{\dot{M}}_{in}$ by a PID control of the evaporator heater, (iv) steadying the condensing surface temperature to a profile $\overline{T}_w(x)$ with the help of the cooling approach described in section 2.3, and (v) using the controllable displacement pump P, through a PID control, to hold the mean inlet pressure fixed at $\overline{p}_{in} = p^*_{in}$. This procedure allows the mean exit pressure $\overline{p}_{exit}$ to freely seek its no fluctuation (abbreviated NF hereafter) steady value $\overline{p}_{exit|NF}$ and defines the no fluctuation (natural) quasi-steady flow with its self-sought pressure difference $\overline{\Delta p}_{|NF} = p^*_{in} - \overline{p}_{exit|NF} \equiv \overline{\Delta p}_{|Na}$ for no fluctuations imposed on the vapor flow at the inlet.

2.4.2 Quasi-Steady Response to Imposed Fluctuations

In this procedure, the mean mass flow rate $\overline{\dot{M}}_{in}$, mean inlet pressure $\overline{p}_{in}$, and the steady cooling conditions remain the same as the ones obtained for the original no-fluctuation flow in section 2.4.1. The compressor continues to remain off. In addition, the bath temperature T_{bath} surrounding the evaporator is also kept constant. The pulsator supplied frequencies for the pressure fluctuations at the inlet are predominantly the frequency (or the rpm) of the motor driving the pulsator and its harmonics. These frequencies (in the inaudible 0 - 20 Hz range) are changed by changing the motor speed (rpm). For present purposes, we will ignore the

harmonics and characterize the pulsations' frequency content by its predominant frequency 'f' as taken from the highest peak in the FFT of $p'_{in}(t)$ (see Fig. 11). The amplitude 'a' of the pressure fluctuations associated with this frequency 'f' is increased by increasing the level of opening of the valve V_P in Fig. 2. When valve V_P is closed, this amplitude 'a' is effectively zero. The above approaches allow for impositions of different inlet pressure fluctuations and the characterization of their amplitude 'a' and frequency 'f' content. These impositions (for the same steady-in-the-mean inlet pressure) may lead to different quasi-steady flows with different steady-in-the-mean exit pressure values. For these new quasi-steady imposed fluctuation (abbreviated IF hereafter) cases, mean value of pressure difference ($\Delta\bar{p}|_{I\text{-}F}$) across the test-section, quasi-steady value of the local heat flux (at HFX-1 in Fig. 1b), test-section thermocouple readings, length x_A of the annular regime (Fig. 1a), etc. are recorded.

3. Results

3.1 No-Fluctuation Condensing Flow Results

As depicted in Figs. 3-5, over the time intervals $t_1 \le t \le t_1^*$, the procedure described in section 2.4.1 is effective in repeatedly achieving a unique no-fluctuation (NF) quasi--steady natural flow for $\overline{\dot{M}}_{in} \approx 1.20$ g/s, steady cooling as specified in section 2.3 (which corresponds to steady wall temperature distributions $\overline{T}_w(x)|_{NF}$ shown in Fig. 4), and $p_{in}^* \approx 142$ kPa. For achieving these flows, the compressor and pulsator were off, and the approximately steady-in-the-mean inlet pressure was set at $p_{in}^* = 142$ kPa. The resulting flow has an effective point of full condensation near the exit and has a flow morphology that changes (with distance from the inlet) from wavy annular to slug/plug to bubbly to all liquid regimes (see the schematic in Fig. 1a and the photographs in Fig. 6a). In Fig. 5, we see that the annular regime differential pressure transducer (DPT–Test Section in Fig. 1a) records the pressure drop (denoted as $\overline{\Delta p}_{0-4|NF}$) with the value of approximately 280 Pa, which is quite small relative to the mean inlet pressure. Also, the heat-flux in the annular region at the HFX-1 location (see Fig. 1b) is $\overline{q''}_{w|NF} \approx 0.59$ W/cm^2 as shown in Fig. 5 and Table 1.

The uniqueness and repeatability of these realizations have been shown elsewhere (see Kivisalu et al. [1]) by a slightly different procedure.

3.2 Quasi-Steady Condensing Flows with Imposed Inlet-Pressure Fluctuations

In the presence of a steady pulsator driving frequency, following the procedure described in section 2.4.2, as the compressor remains off and the pulsator diaphragm frequency is brought from zero to different steady values (3.9 Hz, 5.4 Hz, 10.5 Hz, and 16.1 Hz), new quasi-steady imposed fluctuations cases were achieved. For these quasi-steady cases, the impositions of different time-varying inlet pressures are represented as:

$$p_{in}(t) \equiv \bar{p}_{in}|_{IF} + p'_{in}(t), \quad (1)$$

where

$$p'_{in}(t) \equiv \left[a_{p-in} \sin(2\pi ft)\right] + \text{other terms}. \quad (2)$$

The value of the amplitude $a_{p\text{-}in}$ in Eq. (2) is the amplitude associated with the predominant pulsator frequency 'f' in the fast Fourier transform (FFT) spectrum obtained for the dynamic inlet pressure transducer signal $p_{in}(t)$. Analogous to Eqs. (1)-(2), for any other dynamic variable x(t) associated with these quasi-steady flows, the notations used are:

$$x(t) \equiv \bar{x}|_{IF} + x'(t), \quad (3)$$

where

$$x'(t) \equiv [a_x \sin(2\pi ft)] + \text{other terms}. \quad (4)$$

With the help of the amplitude $a_{p\text{-}in}$ and frequency 'f' used in Eqs. (1)-(2), a representative data-matrix for the inlet pressure fluctuation impositions is shown in Fig. 7a.

The $\dot{M}_{in}(t)$ and $p_{exit}(t)$ results in Fig. 3, the $\overline{T}_w(x)$ results in Fig. 4, and $q''_w(t)|_{HFX\text{-}1}$ and $\Delta p_{0\text{-}4}(t)$ results in Fig. 5 are shown (for data acquisition rate of 0.91 Hz) for lower amplitude (over $t_2 \le t \le t_2^*$, denoted by point P_{21} in Fig. 7a) and higher amplitude (over $t_3 \le t \le t_3^*$, denoted by point P_{31} in Fig. 7a) imposed fluctuation (IF) cases. Henceforth, the representative imposed fluctuation cases (f = 5.4 Hz) denoted by points P_{21} and P_{31} in Fig. 7a are also denoted, respectively, as imposed fluctuation low amplitude (IF-LA) and imposed fluctuation high amplitude (IF-HA) cases. Over $t_2 \le t \le t_2^*$ and $t_3 \le t \le t_3^*$, the time characteristics of the inlet pressure fluctuations and mass flow rates in Fig. 3 are deceptive because the data acquisition rate used is approximately 0.91 Hz. The true nature of the signals is revealed in Fig. 8 onwards where higher speed (2000 Hz) data acquisition is used. In Fig. 8, the dynamic pressure difference ($\Delta p_{om}(t)$) data from the specially designed orifice plate meter (see Fig. 2) are

processed, with the help of computational fluid dynamics (CFD) and empirical correction factors (obtained from suitable calibration experiments), to yield the depicted (and representative) dynamic mass flow rate signals $\dot{M}_{in}(t)$ for the IF-LA case. The empirical corrections obtained from suitable calibration experiments is currently being improved and therefore the data as reported is not reliable with regard to $\dot{M}_{in}{}'(t)$. This improvement is needed because the Coriolis mass flow meter F_c cannot resolve the dynamic nature of the mass flow rate and yields only the time-averaged mean values.

In Figs. 3-5, it is seen that the effects of fluctuations in the vapor flow may (for high amplitude IF-HA cases) or may not (for low amplitude IF-LA cases) significantly change – relative to the natural no-fluctuation (NF) case over $t_1 \le t \le t_1^*$ - the quasi-steady flow variables (e.g. HFX-1 heat-flux $\bar{q}''_{w}|_{HFX\text{-}1}$ in Fig. 4, time-averaged condensing-surface temperatures $\overline{T}_w(x)$ in Fig. 5, flow morphology in Fig. 6b, etc.) associated with changes in condensate thickness, morphology, or motion. For the f = 5.4 Hz case, as the valve V_P in Fig. 2 was gradually opened to increase the pulsation amplitude associated with point P_{21} to that associated with point P_{31} in Fig. 7a, a transition point T_1 (see Fig. 7a) was crossed. A similar transition point is crossed for any other frequency (e.g. T_3 is a representative transition point in Fig. 7a for f = 16.1 Hz). The slope of the heat flux (HFX-1) versus amplitude (of inlet pressure fluctuations) curve in Fig. 7b significantly increases as the transition points are crossed from low amplitude to high amplitude. The transition points T_1, T_3, etc are experimentally located in Fig. 7a. For example, the point T_3 is located with the help of data shown in Fig. 9. This dynamic (acquired at 2000 Hz) heat flux data $q''_w(t)|_{HFX\text{-}1}$ for three different time segments are associated with points P_{23}, T_3, and P_{33} in Fig. 7a. It is clear that the transition value of inlet pressure pulsations' amplitude corresponds to a case where the mean heat-flux shows an in time variation feature that is intermediate between no significant impact (i.e. 16.1 Hz fluctuations are absent) for the low amplitude pulsations case associated with point P_{23} and significant impact (i.e. 16.1 Hz fluctuations are always present in $\bar{q}''_{w}|_{HFX\text{-}1}(t)$) for the high amplitude pulsations case associated with point P_{33}. This intermediate feature over $t_2 \le t \le t_2^*$ in Fig. 9 amounts to occasional appearances and disappearances of the 16.1 Hz frequency peaks in the $q''_w(t)$ data. These transition points in Fig. 7a define a *critical transition amplitude curve* $a^{cr}_{p-in}(f)$ in Fig. 7a (the dotted red curve). In fact the transition points define a narrow band of red curves in Fig. 7a but, for present purposes, it suffices to model them by a single curve. The transition curve in Fig. 7a partitions the inlet pressure pulsations in a *subcritical zone* below the transition curve and a *supercritical zone* above the transition curve. As an example, for the low amplitude IF-LA case associated with point P_{21} in the *subcritical zone* of Fig. 7a, we have $\bar{q}''_{w}|_{HFX\text{-}1} \approx 0.6$ W/cm^2, and for the high amplitude IF-HA case associated with point P_{31} in the *supercritical zone* of Fig. 7a, we have $\bar{q}''_{w}|_{HFX\text{-}1} \approx 2.12$ W/cm^2 (> 250% increase). As a result of the above observations and with the help of the *transition amplitude curve* $a^{cr}_{p-in}(f)$ in Fig. 7a, (with the notations used in Eqs. (1)-(4)) we can say that an inlet pressure pulsation for a fixed $\bar{p}_{in}$ is *subcritical* if

$$\frac{a_{p-in}}{\overline{\Delta p}_{|NF}} < \frac{a^{cr}_{p-in}}{\overline{\Delta p}_{|NF}}, \qquad (5)$$

and is *supercritical* if

$$\frac{a_{p-in}}{\overline{\Delta p}_{|NF}} > \frac{a^{cr}_{p-in}}{\overline{\Delta p}_{|NF}}. \qquad (6)$$

Alternatively, instead of using the inlet pressure amplitude-frequency characterization of fluctuations in Fig. 7a, one could use amplitude-frequency characterizations of fluctuations of a pressure-difference in the annular zone of the flow. For example, by using $x(t) \equiv \Delta p_{0\text{-}4}(t)$ in Eqs. (3)-(4) for characterizing fluctuations in Fig. 7a and defining the critical transition curve as $a^{cr}_{\Delta p\_0-4}(f)$ in the alternate version of Fig. 7a, one could re-state the conditions in Eqs. (5)-(6). In this alternative definition, one could say a pulsation is subcritical or supercritical if

$$\frac{a_{\Delta p\_0-4}}{\overline{\Delta p_{0-4}}_{|NF}} < \frac{a^{cr}_{\Delta p\_0-4}}{\overline{\Delta p_{0-4}}_{|NF}} \quad \text{or} \quad \frac{a_{\Delta p\_0-4}}{\overline{\Delta p_{0-4}}_{|NF}} > \frac{a^{cr}_{\Delta p\_0-4}}{\overline{\Delta p_{0-4}}_{|NF}}. \qquad (7)$$

Note that the amplitude of the inlet pressure fluctuations relative to the mean inlet pressure remains small for both subcritical and supercritical fluctuations and is not a true measure of its impact. It is the fluctuation amplitude's value relative to the small annular zone condenser pressure-difference (as in Eq. 7) that is important.

For brevity, only some of the representative flow realizations from the data matrix in Fig. 7a have been graphically discussed so far. Some of the flow variables associated with the remaining flow cases in the data matrix of

Fig. 7a are briefly reported in Table 1.

For most fully condensing flows discussed above, the overall heat removal rate between the inlet and the effective point of full condensation within the test-section is, approximately, the latent heat released ($\overline{\dot{M}}_{in} * h_{fg}$, since inlet pressure working associated with fluctuations are significantly smaller) plus liquid sub-cooling needed for the non-annular portion of the flow to fully condense. By significant sub-cooling of the liquid below saturation temperature in the non-annular zone, it is meant that the amount of liquid that is below saturation temperature and the amount by which the adjacent condensing-surface temperature is below saturation temperature is significantly higher relative to the annular zone. Therefore, typically, any increase in the heat flow rate over the annular portion x_A of the flow may still accompany a decrease or increase in sub-cooling heat removal rate for the remaining non-annular portion (particularly if this zone is significant in length). In Fig. 6c, for f = 16.1 Hz excitation, the non-annular zone's sub-cooling needs for complete condensation were significantly reduced and, therefore, the non-annular length was significantly reduced (the sub-cooling heat removal rate from TEC-200 and TEC-220 in Fig. 1b were held fixed for this zone). Because of the varying contributions arising from the non-annular zone's sub-cooling needs, one cannot easily develop a generally valid comparison between total heat removed for imposed fluctuation cases and the total heat removed for the corresponding no fluctuation (NF) natural case. In any case, the benefits of the annular zone's supercritical sensitivity to inlet pressure fluctuations can be better exploited in new system designs that involve partially condensing annular flows within the condenser - for such condensers, the amount of vapor condensed within the condenser can vary.

The drastic differences between no fluctuation or subcritical fluctuation cases' quasi-steady flow realizations relative to supercritical quasi-steady flow realizations is apparent in the representative annular zone heat-flux response of Fig. 7b and the reasons are more apparent in the flow morphology videos (not included here) associated with Figs. 6a-6c. These videos show that, for subcritical pulsations, the waves on the annular condensate interface are all moving forward, indicating that the vapor velocity profile does not exhibit any significant flow reversals in the vapor domain. Quite contrary to this, for the larger amplitude supercritical pulsation cases, both forward and backward traveling interfacial waves were observed on the annular condensate (which has a forward average mass flow rate), indicating that the vapor velocity profiles perhaps exhibit significant flow reversals in the vapor domain (particularly in the near interface zone) over the time period of a fluctuation. This phenomenon present in the videos associated with Figs. 6a-6c also has its signature in the IF-HA case's dynamic pressure difference curve $\Delta p_{0-4}(t)$ shown in Fig. 10. The possibility of flow reversal is indicated by the existence of negative values of $\Delta p_{0-4}(t)$ over the IF-HA region in Fig. 10. Perhaps this phenomenon causes a vigorous coupling between the vapor and the condensate motion for the supercritical cases and is accompanied by an annular film thickness profile which also moves up and down at the constant pulsation frequency with a lowered mean film thickness (and a higher mean interfacial shear and heat-flux). In other words, multiple quasi-steady realizations in the supercritical zone are enabled by significant changes in mechanical energy transfer across the interface (this fact was correctly noted in the theory given in Kulkarni et al. [8] but, as discussed later, the computational results on exit pressure fluctuations' effects on mean film thickness had errors).

As a result of the higher heat-flux values and the nature of the steady cooling conditions in section 2.3 (which allow surface temperature variations), following thermal transients, a different steady wall temperature distribution $\overline{T}_w(x)|_{IF-LA} \neq \overline{T}_w(x)|_{IF-HA}$ is achieved, and this is shown in Fig. 4.

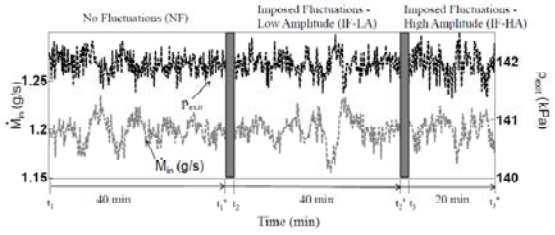

Fig. 3: Inlet mass flow rate, and exit pressure difference for no-fluctuation and imposed-fluctuation flow cases

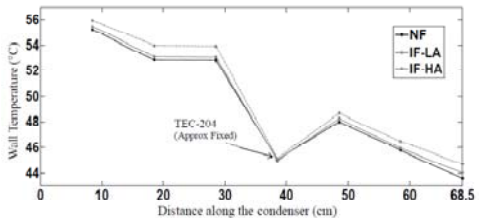

Fig. 4: Steady wall temperature distributions for no-fluctuation and imposed-fluctuation flow cases

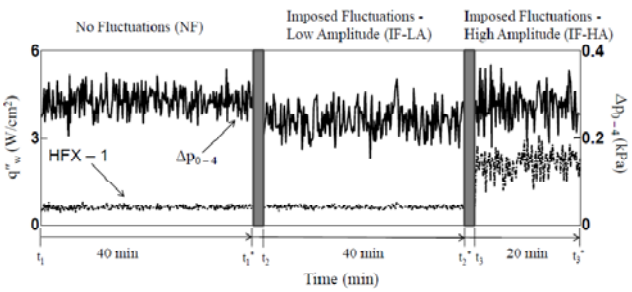

Fig. 5: Heat flux (HFX-1) and test section differential pressure (DPT-Test Section) reading $\Delta p_{0\text{-}4}$ for no-fluctuation and imposed-fluctuation cases

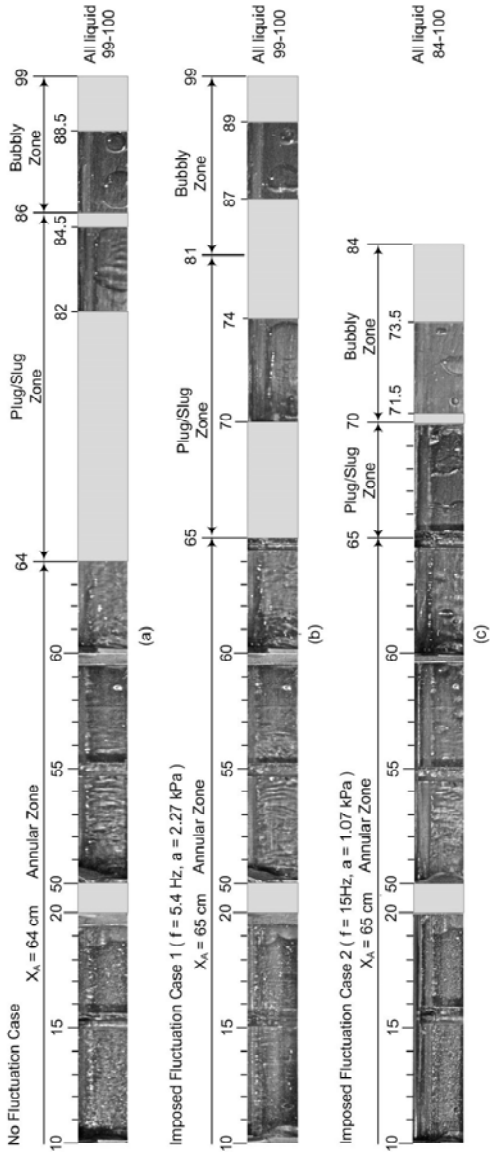

Fig. 6: Liquid-vapor morphology for no fluctuation (NF) and imposed fluctuation cases

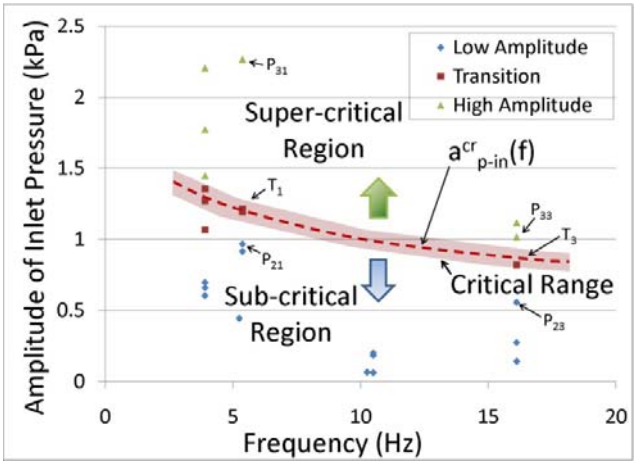

Fig. 7a: Transition map depicting the sub-critical, critical and super-critical region in the amplitude of inlet pressure and frequency domain

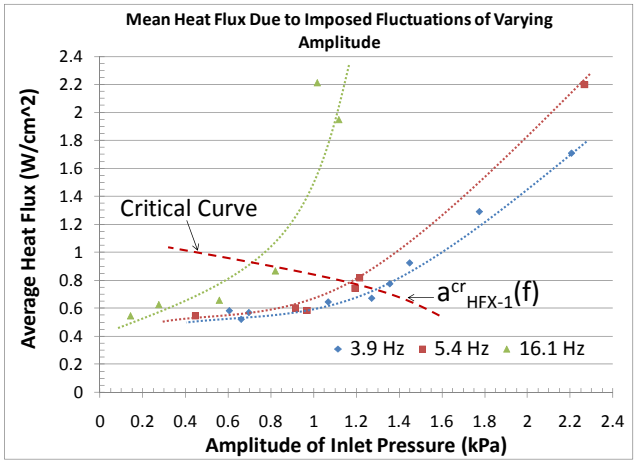

Fig. 7b: Effect of amplitude of inlet pressure fluctuations on the average heat flux at x = 40 cm (HFX – 1)

3.3 The Role of Amplitude-Frequency Content of Fluctuations in Attaining Different Quasi-Steady Flows

To better understand the role of amplitude and frequency content of fluctuations on attaining different steady-in-the mean flows, we look at 5s long dynamic signals (acquired at DAQ rate of 2000 Hz) for: inlet pressure, exit pressure, heat-flux $q''_w(t)|_{HFX-1}$ at the HFX-1 location (see Fig. 1b), and test-section pressure-difference $\Delta p|_{0\text{-}4}(t)$. These dynamic signals are obtained at certain discrete time locations in the time-histories of these variables shown in Figs. 3 - 5. The frequency domain plots (obtained by Fast Fourier Transforms, FFTs) of $[p'_{in}(t) \equiv p_{in}(t) - \bar{p}_{in}]$, $[q''_w(t)|_{HFX-1}]$, $[p'_{exit}(t) \equiv p_{exit}(t) - \bar{p}_{exit}]$, and $[\Delta p_{0\text{-}4}(t)]$ are respectively shown in Figs. 11 - 14. It is clear from Fig. 11 that the pulsator induced frequencies (5.4 Hz and its harmonics) are significantly present for the imposed-fluctuation case but not

for the no-fluctuation cases. As inferred from the heat flux curve in Fig. 12, and also seen in the experimental videos (not shown here), the mean condensate film thickness for the high amplitude imposed fluctuation case oscillates around its mean location with the predominant 5.4 Hz frequency in the heat-flux curve. For the 5.4 Hz high amplitude supercritical fluctuation case, the exit pressure fluctuation amplitude (Fig. 13) relative to the inlet pressure fluctuation amplitude (Fig. 11) is not clearly understood because of the intervening non-annular regimes of the flow and the pressure transducer accuracy limitations.

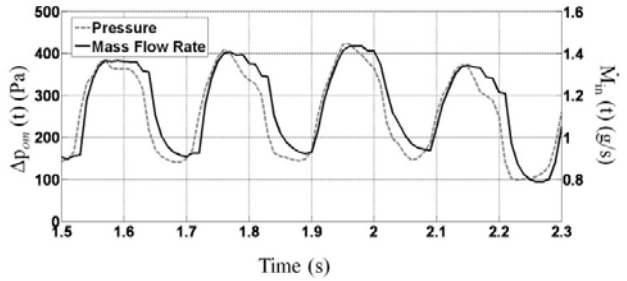

Fig. 8: Orifice plate pressure difference signal $\Delta p_{om}(t)$ and computed mass flow rate $\dot{M}_{in}(t)$ for 5.4 Hz imposed fluctuations

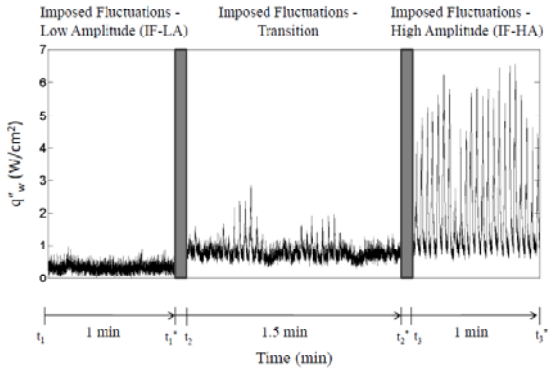

Fig. 9: Dynamic wall heat flux, $q''_w(t)$, for a transition case at 16.1 Hz that compares it with dynamic $q''_w(t)$ for subcritical and supercritical fluctuation cases.

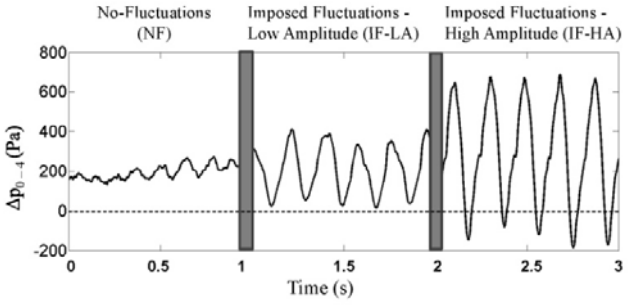

Fig. 10: Dynamic data of the pressure drop in the vapor over the first 40 cm of the annular regime, $\Delta p_{0\text{-}4}$, showing the increase in $\Delta p_{0\text{-}4}$ fluctuations for the LA-IF and HA-IF cases at 5.4 Hz. Note that this pressure drop crosses zero in the HA-IF case.

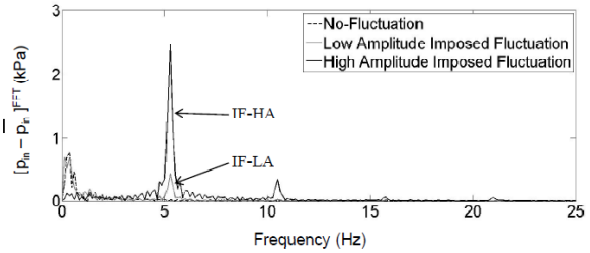

Fig. 11: FFTs of $[\,p'_{in}(t)\,]$ for no-fluctuation and imposed-fluctuation flow cases

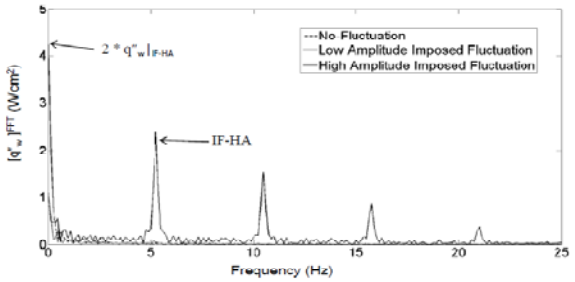

Fig. 12: FFTs of $[\,q''_w(t)|_{HFX\text{-}1}\,]$ for no-fluctuation and imposed-fluctuation flow cases

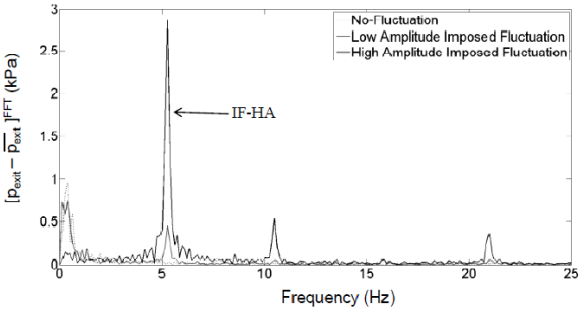

Fig. 13: FFTs of $[\,p'_{exit}(t)\,]$ for no-fluctuation and imposed-fluctuation flow cases

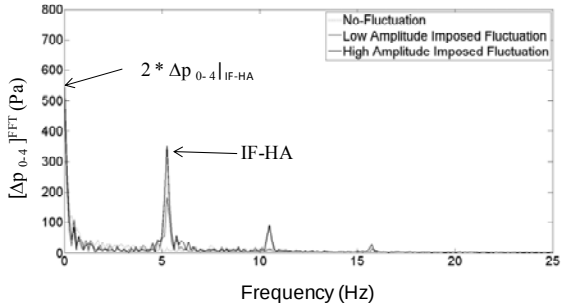

Fig. 14: FFTs of $[\Delta p_{0\text{-}4}(t)]$ for no-fluctuation and imposed-fluctuation flow cases

Our latest computational simulation tool (after correcting for errors in the simulation tool and associated results reported

in Kulkarni et al. [8]) is able to simulate the above described condensing flows for no fluctuation and imposed fluctuation flow categories. These simulations and their comparisons with representative experimental cases will be reported in a separate forthcoming paper.

Table 1: Representative flow results for cases in Fig. 7

Case	Amplitude of inlet pressure a_{pin} (kPa)	Mean Inlet Pressure $\overline{p_{in}}$ (kPa)	Mean Inlet Mass Flow Rate $\overline{\dot{M}_{in}}$ (g/s)	Mean Pressure Difference ** $\overline{\Delta p}$ (Pa)	Mean Wall Temperature - $\overline{T_w(x)}$ x = 8.5 cm (°C)	x = 38.5 cm (°C)	x = 58.5 cm (°C)	x = 88.5 cm (°C)	Mean Heat Flux $\overline{q''_w(x)}$ (W/cm^2)
Natural - No Fluctuations									
NF	0.00	141.85	1.20	20.93	55.44	45.04	45.06	26.55	0.59
Imposed Fluctuations - Frequency = 3.9 Hz									
LA	0.65	141.86	1.20	38.31	55.70	45.00	45.00	27.02	0.63
HA	1.81	141.84	1.20	10.63	55.97	45.17	45.06	26.14	1.27
Imposed Fluctuations - Frequency = 5.4 Hz									
LA	0.45	141.89	1.20	31.06	55.46	45.00	45.93	27.44	0.60
HA	2.27	141.87	1.20	-6.00	55.91	45.15	46.49	24.77	2.12
Imposed Fluctuations - Frequency = 10.5 Hz									
LA	0.13	141.94	1.20	-25.70	54.73	45.01	45.00	24.59	0.57
Imposed Fluctuations - Frequency = 16.1 Hz									
LA	0.14	141.84	1.20	31.25	55.65	45.02	44.50	27.11	0.62
HA	1.07	141.92	1.20	-81.73	55.99	45.02	47.34	21.95	2.14

** Since $\overline{\Delta p}$ values are small relative to the accuracy of APT, the reported values of $\overline{\Delta p}$ may be compared for qualitative purposes but their actual values and signs may not be numerically accurate.

4. Conclusions

- The results reported in sections 3.1-3.3 establish that the multiple quasi-steady flows realized for large amplitude supercritical cases lead to different increased values of heat-fluxes. Furthermore this change is solely due to the large inlet pressure fluctuations and is not affected by the presence or absence of squeezing action from the compressor (details will be reported elsewhere). Computational results (also to be reported elsewhere) supporting the experimental results reported here also finds an error in the elliptic sensitivity results reported in Kulkarni et al.[8]. The corrected results state that exit pressure or exit condensate flow rate fluctuations for partially condensing annular flows cannot lead to different quasi-steady flow realizations unless as a result of this computational imposition from the exit, non-zero fluctuations for the inlet pressure (or inlet flow rate) are necessarily induced (i.e. they are computationally allowed). This means the elliptic sensitivity feature in Kulkarni et al. [8] is incorrect and the true explanation of experimental results in [8] lies not in elliptic sensitivity but in the hitherto unrecognized feature of supercritical parabolic sensitivity (i.e. supercritical inlet pressure fluctuation sensitivity) reported here.
- The above results are consistent with the fact that, under no-fluctuation self-sought pressure-difference conditions for a given mean inlet vapor flow rate and steady cooling conditions, the condenser exhibits only one unique natural quasi-steady flow and associated pressure-difference.
- The reported experimental results demonstrate that significantly different quasi-steady pressure-difference realizations across a shear/pressure driven condenser (as in zero-gravity or in micro-scale applications) are achieved if suitable (but typical) fluctuations are present on a steady-in-the-mean inlet pressure and flow rate. As one traverses from subcritical to supercritical fluctuations, this leads to significantly different quasi-steady flow realizations (arising from different fluctuation amplitude – frequency content of imposed pressure fluctuations) for the same quasi-steady mean mass flow rate, mean inlet pressure and steady cooling. If the resulting effects on flow morphology, local heat transfer rates, and associated significant thermal transients are not taken into account, they may lead engineers to believe that the condenser performance is either non-repeatable or non-deterministic.

Acknowledgment: This work was supported by NASA Grant NNX10AJ59G and NSF Grant CBET-1033591.

References

[1] M. Kivisalu, N. Gorgitrattanagul, S. Mitra, and R. Naik, A. Narain.: "Prediction and Control of Internal Condensing Flows in the Context of their Inlet Sensitivities," submitted (April 14, 2011) for publication in "Microgravity Science and Technology." Paper number: MGST-S-11-00047.

[2] Goodykoontz, J.H., Dorsch, R.G.: Local heat transfer coefficients for condensation of steam vertical down flow within a 5/8-inch diameter tube. NASA TN D-3326 (1966)

[3] Cavallini, A., Zechchin, R.: High velocity condensation of R-11 vapors inside vertical tubes. Heat Transfer in Refrig., 385-396 (1971)

[4] Shah, M.M.: A General Correlation for Heat Transfer during Film Condensation inside Pipes. Int. J. of Heat and Mass Transfer 22, 547-556 (1979)

[5] Cavallini, A., Smith, J.R., Zechchin, R.: A Dimensionless Correlation for Heat Transfer in Forced Convection Condensation. 6th Int. Heat Transfer Conference, Tokyo, Japan (1974)

[6] Mitra, S., Narain, A., Naik, R., Kulkarni, S. D.: A Quasi One-Dimensional Simulation Method and its Results for Steady Annular/Stratified Shear and Gravity Driven Condensing Flows," *International Journal of Heat and Mass Transfer,* **54**, 3761-3776, (2011)

[7] Kurita, J. H., Kivisalu, M., Mitra, S., Narain, A.: Experimental Results on Gravity Driven Condensing Flows in Vertical Tubes, their Agreement with Theory, and their Differences with Shear Driven Flows' Boundary Condition Sensitivities," *International Journal of Heat and Mass Transfer*, **54**, 2932-2951, (2011)

[8] Kulkarni, S. D., Narain, A., Mitra, S., Kurita, J. H., Kivisalu, M., Hasan, M. M.: Flow Control and Heat Transfer Enhancement in Presence of Elliptic-Sensitivity for Shear Driven Annular/Stratified Internal Condensing Flows. in press for publication in Int. J. of Transport Phenomena (2011) Draft available at: http://www.me.mtu.edu/~narain

[9] Wu, H.Y., Cheng, P.: Condensation Flow Patterns in Microchannels. Int. J. Heat and Mass Transfer 48, 286-297 (2005)

[10] Coleman, J.W., Garimella, S.: Two-phase Flow Regimes in Round, Square, and Rectangular Tubes during Condensation of Refrigerant R134a, Int. J. Refrig. 26, 117-128 (2003)

[11] Wedekind, G.L., Bhatt, B.L.: An Experimental and Theoretical Investigation in to Thermally Governed Transient Flow Surges in Two-Phase Condensing Flow. ASME Journal of Heat Transfer 99, 4, 561-567 (1977)

[12] Brutin, D., Topin, F., Tadarist, L.: Experimental study of unsteady convective boiling in heated minichannels. Int. J. Heat and Mass Transfer 46, 2957-2965 (2003)

[13] Kandlikar, S. G.: Fundamental issues related to flow boiling in minichannels and microchannels. Experimental Thermal and Fluid Science, 26, 2-4, 389-407 (2002)